Soft Matter

ARTICLE TYPE

Urea and salt induced modulation of protein interactions: implications for crystallization and liquid–liquid phase separation

– Supplementary information –

M. Madani,[a] T. Hamacher,[a] and F. Platten*[a,b]

Contents

1 Form factor of lysozyme solutions with and without the addition of urea

Figure S1 shows the form factor $P(Q)$ of protein solutions in buffer and in 2 M urea. Both datasets (symbols) agree with each other, and they can be modeled as a prolate ellipsoid (line) with the same ellipsoid parameters, as detailed in Section 2.4 of the manuscript.

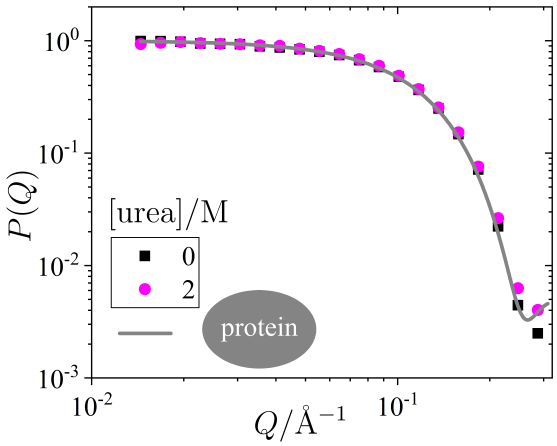

Fig. S 1 Form factor $P(Q)$ of proteins in buffer with and without the addition of 2 M urea (as indicated). Data (symbols, logarithmically binned for clarity) were obtained from the scattered intensity of dilute protein solutions using Equation (1) of the manuscript. Model calculations (line) assume a prolate ellipsoid with a semi-minor axis of 16.0 Å and an axial ratio of 1.5, as described in refs. 1,2.

2 Justification for the Q-range used in the fits

A representative SAXS measurement, including both the full and fitted Q-range, is shown in Figure S2, with the inset displaying the effective structure factor $S_{\text{eff}}(Q)$. Deviations from $S_{\text{eff}}(Q) = 1$ indicate inter-particle interactions, and $S_{\text{eff}}(Q \to 0) > 0$ suggests the presence of net attractive interactions.

The Q-range used for fitting in this study, spanning from 0.03 to 0.31 Å^{-1}, was carefully selected based on the experimental conditions and the specific goals of the analysis. The decision to limit the fitting range was motivated by challenges with background subtraction at very low Q and increased noise at higher Q values, which can compromise the reliability of the data at the extremes.

Moreover, at low Q (i.e., for $Q \lesssim 0.03\,\text{Å}^{-1}$), some SAXS curves exhibit an upturn as Q decreases (see Figure S4a as well as Figures 2a and 3a of the main text, note the logarithmic scale). This behaviour cannot be explained by the Baxter model. A similar, more pronounced upturn was observed in protein solutions near phase separation in ref. 3 and attributed to protein clustering. In that study, the upturn was accounted for by adding a power-law term to the structure factor, which introduced additional free parameters to describe the scattered intensity over the entire Q-range. In contrast, the present study restricts the Q-range for fits based on the Baxter model, minimizing the number of free parameters. However, the analysis could be extended to the full Q-range by incorporating an extra term as in ref. 3. Since the low-Q behaviour would be captured by this additional term, we do not expect the parameters of the Baxter structure factor to be significantly affected by such a modification.

Despite its limits, the Q-range used in the fits is sufficient for reliably determining the second virial coefficient b_2 from SAXS data: As the fitting procedure exploits the Q-dependence of the scattered intensity, the key factor in selecting this range is the

[a] *Faculty of Mathematics and Natural Sciences, Heinrich Heine University Düsseldorf, 40225 Düsseldorf, Germany; E-mail: florian.platten@hhu.de.*
[b] *Institute of Biological Information Processing IBI-4, Forschungszentrum Jülich, 52428 Jülich, Germany.*

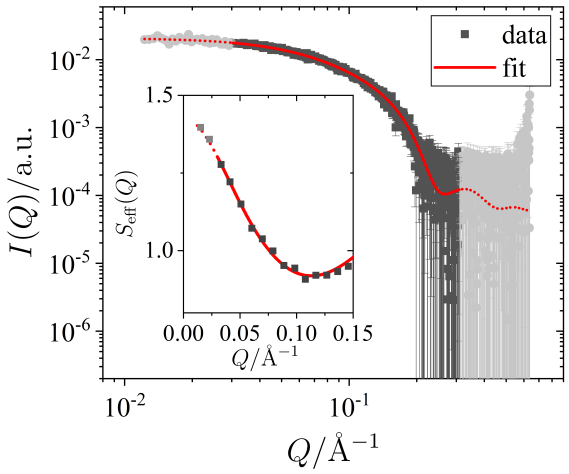

Fig. S 2 Scattered X-ray intensity $I(Q)$ as a function of the scattering vector magnitude Q, with experimental data (symbols) and model fit (solid line) for a representative solution condition: protein concentration $c = 20$ mg/mL, salt concentration 1.5 M, and urea concentration 1.0 M. Black symbols represent the data points used in the fit, while grey symbols at very low and very high Q are excluded from the fitting procedure. The model fit is also shown for the region excluded from the fit (dotted line). The inset shows the effective structure factor $S_{\text{eff}}(Q)$ in the low-Q region, calculated from the data shown in the main figure using Equation (1) of the manuscript. For clarity, the data were binned linearly.

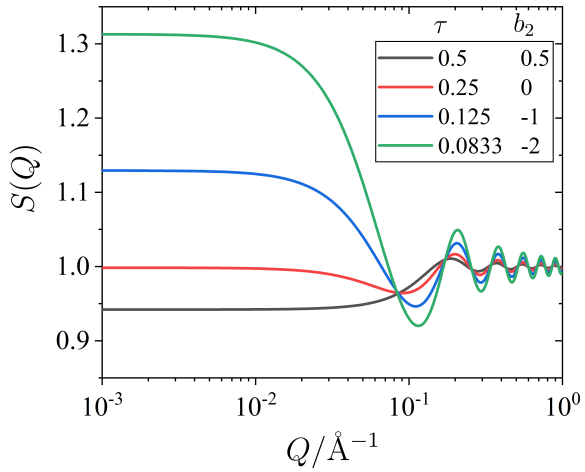

Fig. S 3 Static structure factor $S(Q)$ as a function of the scattering vector magnitude Q, calculated for particles interacting via the adhesive hard-sphere potential. The results are shown for various values of the stickiness parameter τ, which correspond to the indicated values of the normalized second virial coefficient b_2. The calculations use the following parameters: effective particle diameter $\sigma = 36.6$ Å and particle volume fraction $\phi = 0.015$, as considered in the present work.

most significant Q-dependent change just outside the low-Q compressibility plateau (typically reached for $Q \lesssim 0.01\,\text{Å}^{-1}$) extending to the first minimum of $S(Q)$ (typically at $Q \approx 0.12\,\text{Å}^{-1}$). At higher Q-values, the structure factor exhibits oscillations about 1 with decreasing amplitude. These aspects are illustrated in Figure S3, which presents the Baxter model structure factors for various b_2 values, calculated over an extended Q-range using parameters relevant to the present study. The selected Q-range ($0.03 \leq Q/\text{Å}^{-1} \leq 0.31$) captures a significant portion of the curvature of the approach of the structure factor (as Q decreases) from its first minimum to the low-Q plateau, ensuring both the robustness and reliability of the fit.

3 Consistency of the second virial coefficient b_2 inferred from SAXS with independent measurements

The quality of the SAXS data in our study is affected by several inherent limitations. Firstly, the protein concentration used, while suitable for investigating condensation phenomena, does not induce pronounced effects on the structure factor when compared to higher concentrations typically used in SAXS studies. Secondly, the system is prone to crystallization, which limits the duration of SAXS measurements and consequently affects the statistical accuracy of the data.

These limitations raise the question of whether the data quality is sufficient to reliably determine the normalized second virial coefficient b_2, the primary quantity derived from the SAXS data. The experimental protocol and data analysis strategy used in this study align with those employed in previous work (Refs. 1,2), which involved lysozyme solutions at slightly higher protein concentrations and in different solution environments. In those studies, we demonstrated that this approach allows for a reliable quantitative determination of b_2, with results that are consistent with independent, model-free methods.

To further validate this approach for the current system, additional SAXS measurements for lysozyme solutions containing only NaCl (without urea) are presented. Figure S4 illustrates the effect of NaCl concentration on the SAXS of lysozyme solutions at a fixed protein concentration of $c = 20$ mg/mL, without the addition of urea. Panel (a) shows the scattered X-ray intensity $I(Q)$ as a function of the scattering vector magnitude Q, with experimental data (symbols) and model fits (lines). The model fits describe the observed trends accurately. In the inset, the normalized, unshifted data are compared with each other, showing noticeable increase at low Q as salt concentration increases.

Panel (b) presents the static structure factor $S(Q)$ calculated from the model fits shown in (a) and the inset highlights the low-Q differences of the data. Panel (c) illustrates the normalized second virial coefficient b_2 as a function of salt concentration. The data obtained from the current model fits (filled black symbols) are in quantitative agreement with literature values (open coloured symbols), further confirming the reliability of both the experimental protocol and the data analysis strategy. Additionally, the DLVO model calculation (solid line) accurately reproduces the observed trend: an increase in salt concentration leads to a decrease in the second virial coefficient, consistent with the expected screening of electrostatic repulsion.

While the primary challenges with our SAXS data arise from the relatively low protein concentration and limited measurement time, rather than the presence of additives, the methodology used here also provides reliable results for systems containing both

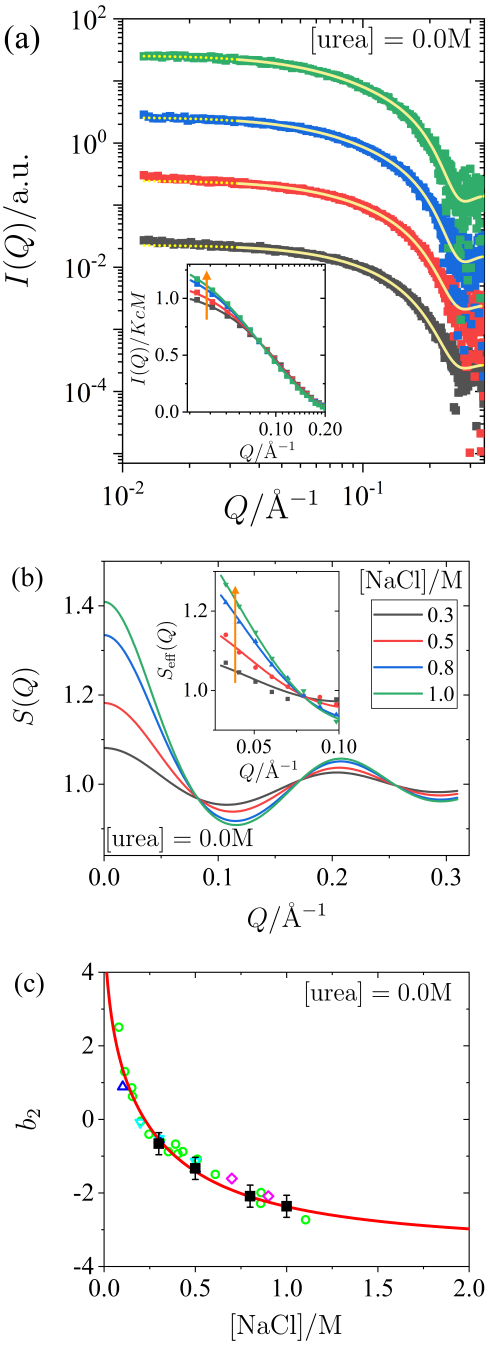

Fig. S 4 Effect of NaCl on the small-angle X-ray scattering of lysozyme solutions at a fixed protein concentration ($c = 20$ mg/mL) without addition of urea, with varying salt concentrations. (a) Scattered X-ray intensity $I(Q)$ as a function of the magnitude of the scattering vector Q, with data (symbols) and model fits (solid lines). The continuation of the model fits into the low-Q region, which is excluded from the fitting procedure, is shown as dotted lines. For clarity, the data and fits are shifted vertically with increasing salt concentration. (Inset) Normalized scattered intensity $I(Q)/KcM$ as a function of Q (data used in the fits, binned for clarity). (b) Static structure factor $S(Q)$ as calculated from the model fits shown in (a). (Inset) Effective structure factor $S_{\rm eff}(Q)$ as a function of Q (data used in the fits, binned for clarity). Vertical arrows indicate increasing salt concentration. (c) Normalized second virial coefficient b_2 of lysozyme solutions as a function of salt concentration. Data are from model fits (filled black symbols) in panel (a) and from the literature (open coloured symbols): △ (Ref. 4), ▽ (Ref. 5), ◯ (Ref. 6), ◊ (Ref. 7). The model calculation (line) is based on DLVO theory, as described in the main text.

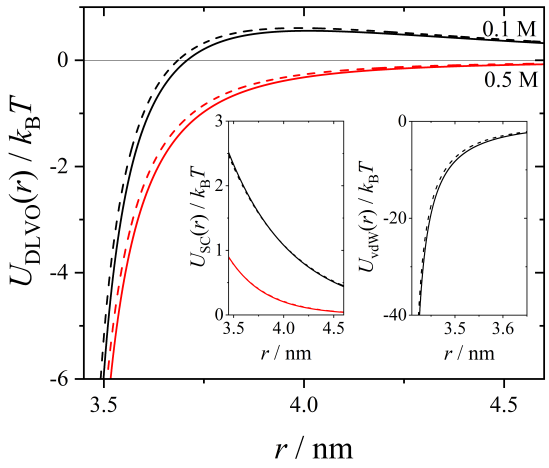

Fig. S 5 DLVO interaction potential $U_{\rm DLVO}(r)$ as a function of the center-to-center distance r between particles with insets showing the screened Coulomb repulsion $U_{\rm SC}(r)$ (left) and the attractive van der Waals contribution $U_{\rm vdW}(r)$ (right) for different salt concentrations 0.1 M (black lines) and 0.5 M (red lines) and urea concentrations 0 M (solid lines) and 2 M (dashed lines). Note the significantly different scales on the axes in the two insets.

urea and salt.

4 DLVO interaction potential in the presence of urea and salt

Figure S5 shows the DLVO interaction potential $U_{\rm DLVO}(r)$ as a function of the center-to-center distance r for two different salt concentrations (represented by the black and red lines) and two urea concentrations (solid and dashed lines). The insets separately display the screened Coulomb potential $U_{\rm SC}(r)$ and the van der Waals potential $U_{\rm vdW}(r)$.

As expected, $U_{\rm SC}(r) > 0$ and $U_{\rm vdW}(r) < 0$, indicating that the screened Coulomb interaction is repulsive, while the van der Waals interaction is attractive. The screened Coulomb potential $U_{\rm SC}(r)$ decays over a characteristic length scale (given by the Debye length κ^{-1}) in the nanometer range, whereas the van der Waals potential $U_{\rm vdW}(r)$ is very short-ranged and diverges as the particles approach contact.

The addition of salt strongly reduces the magnitude of $U_{\rm SC}(r)$ and modifies the Debye length, while it has no significant effect on the van der Waals potential $U_{\rm vdW}(r)$. In contrast, urea addition has little effect on $U_{\rm SC}(r)$ but further shortens the range of $U_{\rm vdW}(r)$.

For low salt concentrations, the DLVO potential $U_{\rm DLVO}(r)$ exhibits a barrier, whereas at higher salt concentrations $U_{\rm DLVO}(r)$ remains negative for all distances. The overall effect of urea addition is primarily dominated by its impact on the van der Waals interaction, leading to a reduction in the range of the DLVO potential.

Notes and references

1 J. Hansen, R. Uthayakumar, J. S. Pedersen, S. U. Egelhaaf and F. Platten, *Phys. Chem. Chem. Phys.*, 2021, **23**, 22384–22394.

2 J. Hansen, J. N. Pedersen, J. S. Pedersen, S. U. Egelhaaf and F. Platten, *J. Chem. Phys.*, 2022, **156**, 244903.

3 M. Wolf, F. Roosen-Runge, F. Zhang, R. Roth, M. W. Skoda, R. M. Jacobs, M. Sztucki and F. Schreiber, *J. Mol. Liq.*, 2014, **200**, 20–27.

4 O. Velev, E. Kaler and A. Lenhoff, *Biophys. J.*, 1998, **75**, 2682–2697.

5 F. Bonneté, S. Finet and A. Tardieu, *J. Cryst. Growth*, 1999, **196**, 403–414.

6 D. F. Rosenbaum, A. Kulkarni, S. Ramakrishnan and C. F. Zukoski, *J. Chem. Phys.*, 1999, **111**, 9882–9890.

7 C. Gögelein, D. Wagner, F. Cardinaux, G. Nägele and S. U. Egelhaaf, *J. Chem. Phys.*, 2012, **136**, 015102.